ELSEVIER

Journal of Nuclear Materials 266–269 (1999) 890–895

journal of nuclear materials

Modeling of neutral particle distributions at the L to H transition in DIII-D

L.W. Owen [a,*], B.A. Carreras [a], R. Maingi [a], P.K. Mioduszewski [a], T.N. Carlstrom [b], R.J. Groebner [b]

[a] *Oak Ridge National Laboratory, P.O. Box 2009, Oak Ridge, TN 37831-8072, USA*
[b] *General Atomics, P.O. Box 85608, San Diego, CA 92186-9784, USA*

Abstract

In order to study possible effects of neutrals on the power threshold for transition from L-mode to H-mode confinement in DIII-D, the problem of reconstructing neutral particle distributions inside the separatrix from available edge, scrape-off layer, and divertor plasma diagnostic data is addressed. Neutral particle profiles in the shear layer are reconstructed primarily with the DEGAS code using plasma parameters obtained by fitting discharge data with the B2.5 code. A series of discharges in which the ion grad B drift direction is toward the X-point is analyzed. For reversed B_t, the L to H transition power threshold is 2–4 times higher than normal B_t discharges at the same density: one discharge of this type is analyzed. The variation of the L–H transition power threshold divided by the density is seen to be correlated with the neutral density scale length in the shear layer for both directions of the magnetic field. Radial and poloidal neutral particle profile results for three low density discharges in which the L–H transition power threshold varies from 1.3 to 5.3 MW are presented.

Keywords: Two dimensional modeling; Atomic density; DIII-D; Charge-exchange neutrals; Divertor modeling; Neutral transport; Effective particle confinement; Power balance; SOL modeling; Transport barrier

1. Introduction

One of the characteristic properties of the transition from the low confinement mode (L-mode) to the high confinement mode (H-mode) is a power threshold, which from the early experiments was observed to scale directly with the line-averaged density and the magnetic field for single null divertor discharges with the ion grad B drift toward the X-point [1]. From early experiments it was also shown that access to the H-mode requires reduction in recycling through careful wall conditioning [2]. Both wall conditioning and plasma configuration effects were seen [3] to cause significant changes in the L–H power threshold. A possible mechanism for the observed effects of wall condition on the threshold is the coupling of the neutral dynamics to the transition mechanism.

The power threshold for the transition from L-mode to H-mode ($P_{L–H}$) can be affected by the transport of neutral particles in the shear layer through flow damping by charge-exchange (CX) friction, changes in the level and topology of the $E \times B$ flow shear, and modification of the energy, particle, and momentum balances. The threshold can also be affected by changes in density, temperature, and radial electric field profiles that result from neutral transport in the divertor, edge, and scrape-off layer (SOL). Since direct measurements of neutral density and temperature profiles inside the separatrix are not yet available, they must be inferred through modeling.

Data from lower single-null (LSN) DIII-D discharges in which the ion grad-B drift is towards the X-point are analyzed for a range of operating conditions and line-averaged densities. These conditions are obtained by

* Corresponding author. Tel.: +1-423 574 0634; fax: +1-423 574 0634; e-mail: owenl.@feda01.fed.ornl.gov

0022-3115/99/$ – see front matter
PII: S0022-3115(98)00881-2

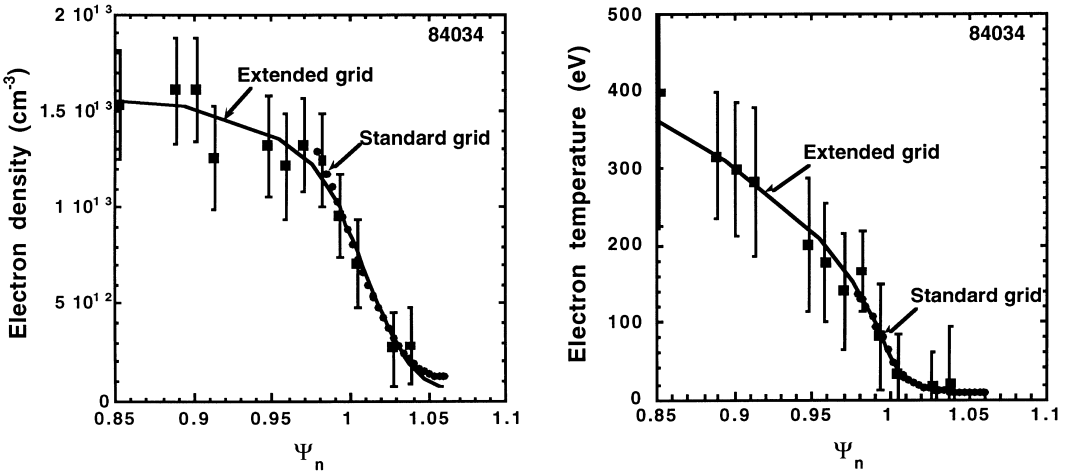

Fig. 1. Electron density and temperature profiles along the Thomson chord (as well as the other core and divertor diagnostic data fits) show no significant differences between the standard and extended grid simulations for Shot 84034.

active control of the neutrals through gas fueling, pumping, and X-point position, as well as operation in the standard (reference) configuration. Analysis results for a single LSN discharge 92089 with reversed B_t (ion grad-B drift away from the X-point) are presented. Typically available diagnostic data include electron density and temperature profiles from Thomson scattering, ion temperatures from CER spectroscopy, divertor D_α, IRTV, and Langmuir probe data, 2-D radiation profiles, and neutral pressures at various points in the vessel. The data are fitted with the B2.5 plasma transport code [4], and the resulting plasma parameters are used in the DEGAS code [5] to calculate core fueling rates and neutral profiles. The calculations are iterated until the core fueling rate from divertor recycling, Γ_{fuel}, computed with DEGAS, is consistent with the integrated ion flux across the separatrix, Γ_{core}, from B2.5. The details of the analysis procedure are given in Ref. [6].

The analysis is focused on reconstructing the neutral profiles in the shear layer just before the L to H transition. Since the shear layer can extend several centimeters into the core plasma (inside the separatrix), it is desireable to fit the plasma parameters in this region in order to establish continuity of the profiles and their respective gradients. The details of how we do this with stand-alone B2.5 calculations are discussed in Section 2. A qualitative discussion of the power and temperature dependence of CX rates and, by implication, corresponding effects on poloidal rotation damping is presented in Section 3. Some general results from the plasma/neutral transport calculations, and a comparison of three low density discharges among which $P_{\text{L–H}}$ varies by a factor of 3, are given in Section 4.

2. Plasma transport simulations in the shear layer

In the procedure adopted for this work, the analysis required to assess possible effects of neutrals on the L–H transition power threshold involves two steps. The first step, which is the focus of this paper, consists of fitting the discharge data and generating 2-D distributions of the neutral particle parameters with iterative B2.5/DEGAS calculations. The second part of the analysis involves evaluation of parameters that may characterize the role of neutrals in the transition; details and results for normal B_t discharges are given in Ref. [7].

The version of the edge transport code that we use, B2.5, contains a semi-analytic multiple-species neutrals model that includes the transport of molecules, Franck–Condon atoms, and energetic reflected atoms, as well as an approximation for CX neutrals [8]. This model has been compared with coupled B2/DEGAS calculations with good agreement over a broad range of plasma conditions. While the neutral transport in the divertor region is well described by the semi-analytic model, it is not possible in general to accurately describe with such a model the multiple wall reflections and CX events that result in core fueling by recycling neutrals. Consequently, stand-alone B2.5 calculations are usually limited to a domain that extends only a centimeter or so into the core plasma, i.e., regions where the plasma transport is dominated by parallel flow.

In this section we describe a method of performing stand-alone edge transport calculations across the shear layer (the edge plasma layer extending several centimeters inside the separatrix). This method involves the use of a positive convective term in the radial particle flux that fuels this edge plasma layer with ions from deeper inside the core, thereby enabling fits to the electron

density profile and the electron and ion temperature profiles across this edge region. It should be emphasized that the positive convective (anti-pinch) term in this context is merely a tool to enable fueling of the edge plasma and profile fitting in all regions. A strong radial dependence of the particle diffusivity could also serve this purpose.

Since its presence changes the mix of conductive and convective radial transport, we have extensively tested the effect of the convective term on the edge transport solution and on the results from the neutral transport. For several discharges, we have compared the results from the standard grid simulation, with the inner boundary at normalized magnetic flux $\Psi_n = 0.98$ and no convective term, to the corresponding simulation including the convective term with the boundary at $\Psi_n = 0.85$ (extended grid). In all cases, we have obtained comparable fits to the SOL and divertor data. The particle diffusivities are smaller in the extended grid case due to the presence of the convective term. Otherwise, the parameters in the edge transport calculation are approximately the same as for the standard grid. For example, the electron density and temperature profiles for standard and extended grid simulations, displayed in Fig. 1 for Shot 84034, show no significant differences over the common region. The corresponding fits to the ion temperature and divertor D_α and IRTV data for the two cases were indistinguishable in the common region and are not shown.

3. Power/temperature dependence of charge-exchange

Amplification of the $E \times B$ flow shear through the Reynolds stress drive is thought to be the mechanism responsible for the L–H transition [7]. If the pressure gradient term is small compared to the ion velocity terms in $V_{E \times B}$, the transition condition is rather simple. To have a transition, the Reynolds stress flow amplification must dominate over all damping terms. One of the possible roles of neutrals in impeding the transition, an enhanced flow damping due to CX friction, increases the power threshold. This is a general result that carries over to all models that incorporate the $E \times B$ shear flow suppression of turbulence as the basic transition mechanism.

The CX damping is strongest near the X-point, where the core fueling from divertor recycling peaks (see discussion in Section 4). In this section we examine the implications of the temperature (or power) dependence of the CX rate coefficients, $\langle \sigma v \rangle_{cx}$, for the local rates, the integrated core CX rates, and the associated flow damping. The DEGAS neutral transport calculations of the ratio of the volume-integrated core CX rate to the core ionization (fueling) rate fall on a smooth curve, suggesting that this ratio could be described for all input power levels by the ratio of the rate coefficients at some average temperature. Fig. 2(a) shows that the ratio $P_{sep}/\langle n_e \rangle$ is almost perfectly correlated with the average of the electron and ion temperatures to the 3/2 power at the $\Psi_n = 0.9$ flux surface. Here P_{sep} is the power crossing the separatrix and is distinguished from P_{L-H} since these results hold for both L-mode and H-mode. It is seen in Fig. 2(b) that the DEGAS calculations (points with 'error' bars) are very well reproduced by a constant (of order unity) times the ratio of the reaction rates. The temperatures at which the rate coefficients are evaluated for each power are taken from Fig. 2(a). The utility of this result can be described as follows. If the core ionization rate is known or esti-

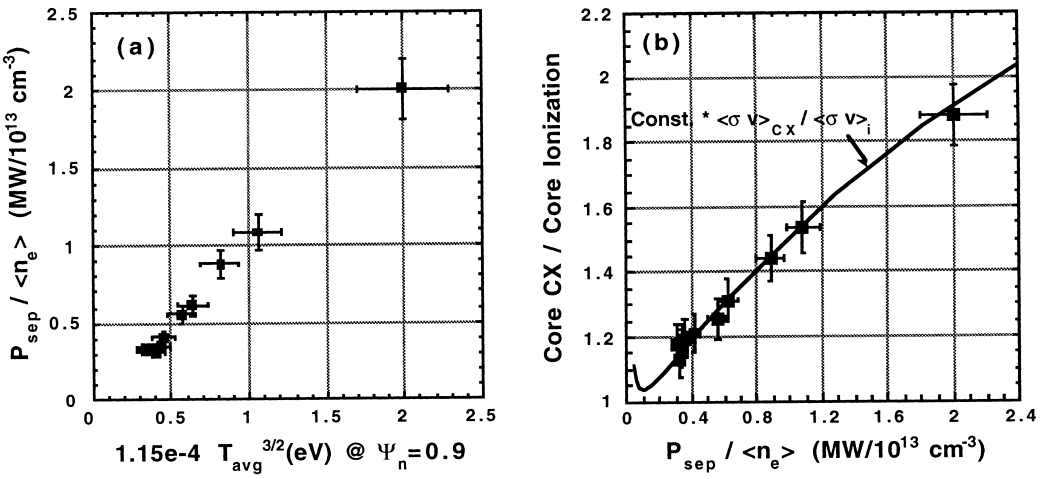

Fig. 2. (a) The ratio of $P_{sep}/\langle n_e \rangle$ and the average of the electron and ion temperatures to the 3/2 power at $Y_n = 0.9$ are linearly related. (b) The ratio of core CX to core ionization can be estimated from the ratio of the reaction rates and the results shown in (a). The 10% error bars shown on the points computed with DEGAS are approximate.

mated from the measured dN_e/dt, for example, then the level of core CX can be estimated using measured core temperature profiles.

These results also have implications for flow damping and the power required for the L–H transition. If we assume that the core particle confinement time scales inversely with $P_{sep}^{1/2}$ in L-mode (there is some indication of this in the calculations presented in Section 4), then the results in Fig. 2 indicate that the core CX rate (and the associated flow damping) should vary as $P_{sep}^{3/2}$. This means that the CX flow damping may increase stronger than linearly with power as the power is ramped towards the transition threshold.

4. Analysis and discussion

We have analyzed a total of 12 DIII-D discharges at time slices in the L-mode phase that are typically 15–20 ms before the L to H transition. For each of the discharges, the free parameters of the plasma transport code (particle and heat diffusivities, convective velocity, plate and/or wall recycling coefficients, etc.) were varied to fit to the diagnostic data. The two free parameters (particle diffusion coefficient and convective velocity) in the radial particle flux for the extended grid simulations were constrained in most of the cases by first fitting the data with $V_{conv} = 0$ (standard grid). This constraint was relaxed for the analysis of the reversed B_t discharge in order to satisfy power balance. The typical quality of the agreement of the data and the calculations can be seen in Fig. 1. After fitting the edge profile, divertor, and radiation data, the neutral transport calculation is performed with the background plasma parameters from B2.5. The Γ_{core} from the plasma transport calculation and Γ_{fuel} from DEGAS are compared via the particle balance equation; if they are not consistent, the process is repeated with different transport and/or recycling coefficients. This procedure typically requires four or five iterations of the plasma and neutral transport calculations to obtain Γ_{core} and Γ_{fuel} that are consistently within 10%.

Agreement of the core fueling rate from DEGAS with the integrated particle flux crossing the separatrix from B2.5 (as determined from the core particle balance equation, $dN_{core}/dt = \Gamma_{fuel} + \Gamma_{NBI} - \Gamma_{core}$, where Γ_{NBI} is the beam fueling rate) is the key requirement for establishing consistency of the plasma and neutral transport. The steady-state core fueling rate from divertor recycling is shown in Fig. 3(a) for the discharges analyzed. It is seen that for normal B_t, the core ionization or fueling rate is approximately linear with density. A linear fit to the points gives a low-power L-mode particle confinement time, $\tau_p = N_{core}/\Gamma_{core}$, of 165 ms for the normal B_t discharges. For the reversed B_t discharge τ_p is smaller than that for normal B_t by approximately the square root of the average ratio of the threshold powers. (This ratio is 2–4 for $\langle n_e \rangle$ about 2.5×10^{13} cm^{-3}.) For the normal B_t discharges the range of measured P_{L-H} and the scatter in the Γ_{core} and Γ_{fuel} values does not permit an unambiguous determination of the power dependence of τ_p.

Since the neutral distributions are two dimensional (toroidal symmetry assumed), it is useful to define a poloidally averaged radial length parameter for neutral particle-related quantities (neutral densities and temperatures, CX rates, ionization rates, etc.) in the shear layer,

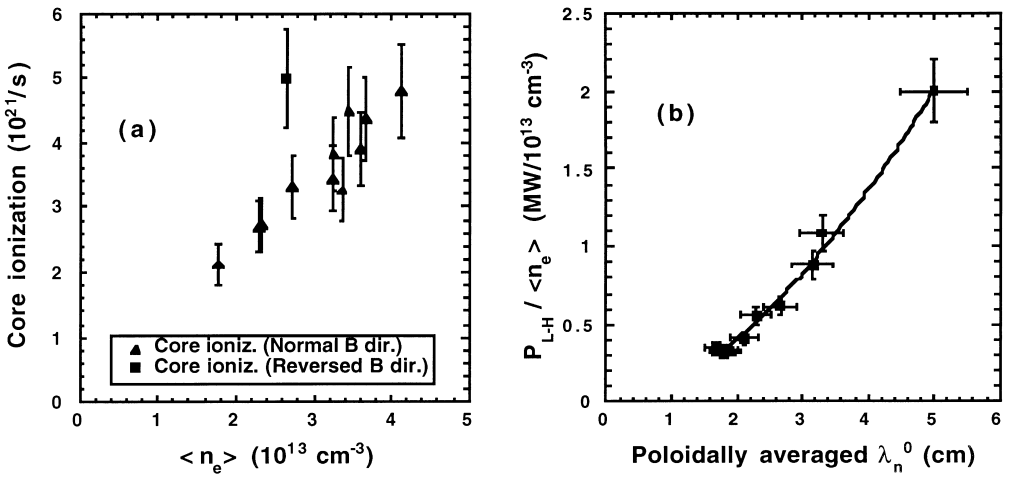

Fig. 3. (a) The core fueling rate from divertor recycling increases approximately linearly with density for the normal direction of the toroidal magnetic field. (b) The ratio of the L–H transition power threshold to the density is well correlated with neutral density scale length in the shear layer. Both normal and reversed B_t thresholds are described by a single power law.

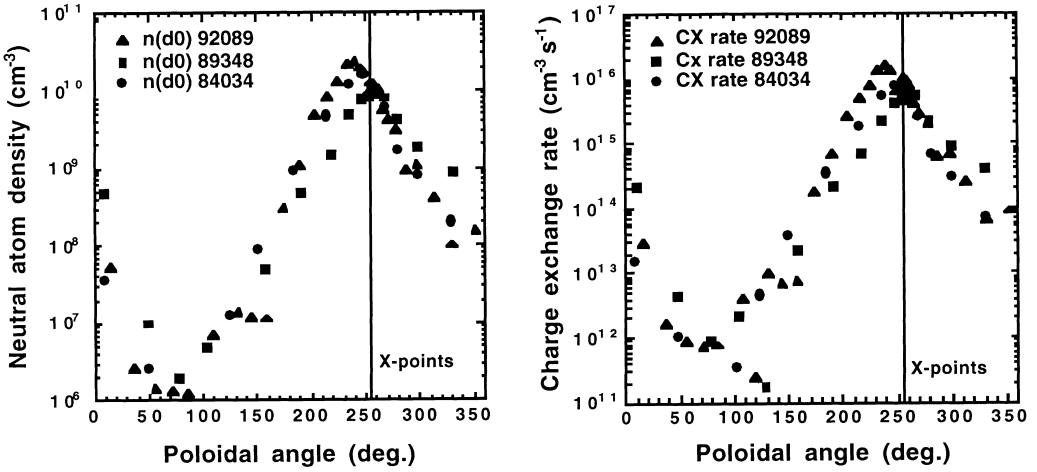

Fig. 4. Poloidal distributions of neutral density and CX rate just inside the separatrix for Shots 92 089, 89 348, and 84 034 indicate that the CX (and core fueling) from divertor recycling peak near the X-point.

$$\rho = [r_{\rm sep} - r]_{\rm avg} = \frac{\sum_\theta [r_{\rm sep}(\theta) - r(\theta)] n_0(r,\theta) V(r,\theta)}{\sum_\theta n_0(r,\theta) V(r,\theta)},$$

where θ denotes the cell number, r is measured from the minor axis to the cell center, $r_{\rm sep}$ is the radial distance from the minor axis to the separatrix segment nearest to the cell, n_0 is the neutral density, and V is the cell volume. With radial distance inside the separatrix measured in this way, poloidally averaged one dimensional profiles can be fitted with exponentials and characterized by scale lengths in the shear layer. With the scale length deduced in this way, we see in Fig. 3(b) a strong correlation of the ratio of the L to H transition threshold power to the average density, $P_{\rm L-H}/\langle n_{\rm e}\rangle$, with neutral density scale length, λ_n^0, inside the separatrix. (For constant magnitude of the toroidal magnetic field, the quantity $P_{\rm L-H}/\langle n_{\rm e}\rangle$ should be essentially a function only of the 'hidden' parameters controlling the transition.) The solid curve is a power law fit, $(\lambda_n^0)^{7/4}$, and describes the simulation results for both directions of the toroidal magnetic field. An equally strong correlation of $P_{\rm L-H}/\langle n_{\rm e}\rangle$ with the CX rate radial scale length is also seen; the principal difference is that the scale length of CX rate is larger than that of neutral density, as discussed in Section 3.

Among the normal $B_{\rm t}$ discharges analyzed, the variation in $P_{\rm L-H}$ is only from about 1–2.5 MW, with the two pumped shots having the largest $P_{\rm L-H}$ [7]. In order to minimize effects of the density dependence of $P_{\rm L-H}$, we have chosen three discharges having approximately the same line-averaged density for a more detailed presentation of results. These discharges are 84034, 89348 (pumped), and 92089 (reversed $B_{\rm t}$). The respective densities in units of 10^{13} cm^{-3} ($P_{\rm L-H}$ in units of MW) are 2.3 (1.3), 2.3 (2.5), and 2.6 (5.3). The magnitude of $B_{\rm t}$ is 2.1 T for all discharges analyzed here. Further motivation for examining low density discharges in detail is found in results from the Japan Atomic Energy Research Institute Torus-60 Upgrade (JT-60U) [9], in which an analysis similar to the one presented here indicated that, for low density plasmas, neutrals could have substantial influence on the L–H transition threshold [10,11].

For low density discharges in DIII-D, the power across the separatrix, $P_{\rm L-H}$, as determined from the core power balance equation, is typically larger than that which is measured by the divertor/SOL diagnostics. For the three discharges discussed in this section about 30% of $P_{\rm L-H}$ is contained in core CX losses, heat flux to the center post, SOL CX losses, etc. that are not directly measured by the diagnostics. Consequently, in the analyses presented here we have demanded that 70% of $P_{\rm L-H}$ cross the separatrix in the B2.5 simulations. In order to satisfy this requirement it is sometimes necessary to adjust the relative positions of the Thomson chord data and the separatrix, $\Delta\Psi_{\rm n}$, as determined from the EFIT code [6]. In the case of Shot 92 089 $\Delta\Psi_{\rm n} = 0.025$ was required to simultaneously fit all of the data. The necessity for this adjustment may be due in part to the presence of radial drifts that are not included in the models. Excellent fits are obtained with the B2.5 code to the Thomson scattering, CER, and divertor data for the three discharges. Electron–ion temperature equilibration in the core is sufficiently complete for the $T_{\rm e} = T_{\rm i}$ approximation at $\Psi_{\rm n} = 0.9$, assumed for the discussion in Section 3, to be good. The effects of this on CX rates are discussed below.

In assessing possible effects of neutrals on the L to H transition threshold it is also instructive to look at the poloidal dependence of the neutral distributions. The

poloidal distributions of neutral density and CX rate just inside the separatrix are shown in Fig. 4. Since $\langle \sigma v \rangle_i$ is not a strong function of the plasma parameters in the separatrix density and temperature regimes of these three discharges, the corresponding ionization rate distributions follow the neutral density very closely and show that the core fueling from divertor recycling is strongly peaked near the X-point. It should be noted that the distribution for the pumped discharge is significantly broader than the others; this is probably due to the effects of recycling from the top of the bias ring [12] into the region below the outer midplane. For the discharges analyzed in this study, we have not seen a strong correlation of the neutral density at the separatrix and P_{L-H}, even though the correlation with neutral density and CX rate scale lengths is extremely good. The CX rate curves in Fig. 4 illustrate the point made in Section 3 that the neutral density alone does not determine the CX damping rate in the shear layer. The peak neutral density for 84034 is almost a factor of 2 larger than that for 89348, but the CX rate is only 15% larger. This is, of course, due to the temperature dependence of the quantities involved.

To conclude, there is a strong correlation between neutrals at the plasma edge and the power threshold for L to H transitions in DIII-D. A mechanism possibly responsible for the neutrals effects on the transition threshold is an increase in the damping of the $E \times B$ shear flow by neutral/main ion CX friction.

Acknowledgements

This is a report of work supported by the Office of Fusion Energy, US Department of Energy under contract DE-AC05-96OR22464 with Lockheed Martin Energy Research Corporation and DE-AC03-89ER5114 with General Atomics. We gratefully acknowledge M.E. Rensink and B. Braams for letting us use their computer codes, and K.H. Burrell, P.H. Diamond, J.T. Hogan and M.R. Wade for multiple discussions on the neutrals effects.

References

[1] K.H. Burrell, S.L. Allen, G. Bramson et al., Proceedings of the 12th International Conference on Plasma Physics and Controlled Nucl. Fusion Research, vol. 1, International Atomic Energy Agency, Vienna, 1988, pp. 193–205.
[2] The ASDEX Team, Nucl. Fusion 29 (1989) 1959.
[3] T.N. Carlstrom, P. Gohil, J.G. Watkins, K.H. Burrell, S. Coda, E.J. Doyle, R.J. Groebner, J. Kim, R.A. Moyer, C.L. Rettig, Plasma Phys. Contr. Fusion 36 (1994) A147.
[4] B.J. Braams, Contrib. Plasma Phys. 36 (1996) 276.
[5] D.B. Heifetz, D. Post, M. Petravic, J. Weisheit, G. Bateman, J. Comp. Phys. 46 (1982) 309.
[6] L.W. Owen, R. Maingi, D.K. Lee, P.K. Mioduszewski, D.R. Baker, D.L. Hillis, J.T. Hogan, G.L. Jackson, M.R. Wade, J. Nucl. Mater. 220–222 (1995) 315.
[7] B.A. Carreras, L.W. Owen, R. Maingi, P.K. Mioduszewski, T.N. Carlstrom, R.J. Groebner, Phys. Plasmas 6 (1998) 623.
[8] R. Maingi, J.T. Hogan, L.W. Owen, P.K. Mioduszewski, M.E. Rensink, J.G. Gilligan, O.E. Hankins, K.A. Werley, Nucl. Fusion 34 (1994) 283.
[9] M. Shimada and the JT-60U Team, Proceedings of the 14th International Conference on Plasma Physics and Controlled Nuclear Fusion Research, vol. 1, International Atomic Energy Agency, Vienna, 1992, pp. 55–57.
[10] K. Tsuchiya, H. Takenaga, T. Fukuda, Y. Kamada, S. Ishida, M. Sato, T. Takizuka, Team JT-60U, Plasma Phys. Contr. Fusion 38 (1966) 1295.
[11] T. Fukuda, M. Sato, T. Takizuka, K. Tsuchiya, Y. Kamada, H. Takenaga, and the JT-60U Team, Proceedings of the 16th IAEA Fusion Energy Conference, International Atomic Energy Agency, Vienna, vol. 1, 1966, pp. 857–866.
[12] M.A. Mahdavi et al., J. Nucl. Mater. 176&177 (1990) 32.